scientific reports

Check for updates

OPEN

Eosinophils mitigate intestinal fibrosis while promoting inflammation in a chronic DSS colitis model and co-culture model with fibroblasts

Inge Jacobs[1,2], Sara Deleu[2], Bo-Jun Ke[2], Jonathan Cremer[1], Ellen Dilissen[1], Gert De Hertogh[4], Tobie Martens[2,5], Pieter Vanden Berghe[2,5], Gianluca Matteoli[2], Séverine Vermeire[2,3], Christine Breynaert[1,6], Tim Vanuytsel[2,3,7] & Bram Verstockt[2,3,7]✉

Eosinophils were previously reported to play a role in intestinal inflammation and fibrosis. Whether this is as a bystander or as an active participant is still up for debate. Moreover, data describing a causal relationship between eosinophils and intestinal fibrosis are scarce. We here aimed to elucidate the role of eosinophils in the pathogenesis of intestinal inflammation and fibrosis. Therefore, we stimulated fibroblasts with (active) eosinophils or with Eosinophil Cationic Protein (ECP), and assessed fibroblast activation via flow cytometry and immunocytochemistry. We observed decreased fibroblast activation when fibroblasts were co-cultured with active eosinophils or after stimulation with ECP in comparison to monoculture conditions, but not in case of co-culturing with inactivated eosinophils. Furthermore, eosinophil depletion in a RAG$^{-/-}$ chronic DSS colitis model resulted in decreased inflammation, but increased development of fibrosis. In this model, we could show increased expression of the anti-inflammatory protein IL-10 and the pro-fibrotic factors IL-1β, FGF-21 and TGF-β3 in the eosinophil-depleted mice compared to the control mice. In conclusion, our in vitro data revealed an anti-fibrotic role for eosinophils. In line, in a chronic murine colitis model, we observed a pro-inflammatory, but an anti-fibrotic, role for eosinophils. Furthermore, we identified an increased presence of anti-inflammatory and pro-fibrotic cytokines in the eosinophil depleted group.

Keywords Eosinophils, Pro-inflammatory, Anti-fibrotic, In vitro co-culture, DSS colitis model

Crohn's disease (CD) is a chronic inflammatory bowel disorder characterized by a relapse-remitting inflammatory profile, in which tissue remodeling is common and fibrotic strictures are a feared complication[1]. These strictures arise from excessive fibroblast activation and differentiation towards myofibroblasts, leading to excessive extracellular matrix (ECM) deposition, thickening of the muscularis propria[2], narrowing the lumen and the necessity for surgical intervention in more than 50% of CD patients[3]. Even though several risk factors contributing to this process have been identified, the detailed mechanistic pathway has yet to be elucidated.

Previously, eosinophils have been identified as possible pro-inflammatory cells[4]. In a clinical setting, eosinophil infiltration in the lamina propria is a common finding in active UC and was therefore also included in the original histological score for UC by Geboes et al.[5–7]. Eosinophils are filled with eosinophil-specific mediators such as eosinophil cationic protein (ECP), eosinophil peroxidase (EPX), eosinophil derived neurotoxin (EDN) and eosinophil major basic protein (MBP)[8]. All of these mediators have previously been implicated in inflammation[9–11]. In other disease areas, IL-5 inhibition (e.g. by benralizumab, mepolizumab or reslizumab)

[1]Department of Microbiology, Immunology and Transplantation, Allergy and Clinical Immunology Research Group, KU Leuven, Leuven, Belgium. [2]Translational Research Center for Gastrointestinal Disorders (TARGID), KU Leuven, Leuven, Belgium. [3]Department of Gastroenterology and Hepatology, University Hospitals Leuven, LeuvenHerestraat 49, Belgium. [4]Department of Imaging and Pathology, Translational Cell & Tissue Research, KU Leuven, Leuven, Belgium. [5]Cell and tissue Imaging Cluster (CIC), KU Leuven, Leuven, Belgium. [6]Department of General Internal Medicine, University Hospitals Leuven, Leuven, Belgium. [7]These authors jointly supervised: Tim Vanuytsel and Bram Verstockt. ✉email: bram.verstockt@uzleuven.be

decreased eosinophil counts and overall type 2 immune response, with e.g. a decreased overall disease severity in patients with eosinophilic asthma[12]. Likewise, clinical benefit of benralizumab in active UC has been reported[13]. Preclinical models further demonstrated a pro-inflammatory role for eosinophils in intestinal inflammation: MBP knock-out mice are protected against colitis in an oxazolone colitis model[14], and EPX knockout mice show less active colitis in a DSS colitis model[15]. Also in vitro studies have shown that activating eosinophils and co-culturing them with fibroblasts led to the release of the pro-inflammatory cytokines TNF-α and IL-6[16].

Besides inflammation, eosinophils have also been implicated in fibrosis although in other organs than the gut. Murine models exhibiting eosinophil depletion significantly reduced hepatic, pulmonary and renal fibrosis[15,17,18]. Moreover, anti-IL-5 injections decreased intestinal eosinophils, resulting in reduced radiation induced fibrosis[17]. EPX knockout resulted in decreased renal fibrosis in a unilateral ureteral obstruction model, mediated by a decrease in collagen I deposition and α-SMA expression, indicative of decreased active fibroblasts and a pro-fibrotic role for EPX[15]. Additionally, the exposure of the eosinophil-specific mediators EPX and MBP to pulmonary epithelial cells increased production of the pro-fibrotic factors *TGF-β*, *epidermal growth factor receptor*, *platelet derived growth factor* and *tenascin*[18].

Current evidence therefore points towards a potential involvement of eosinophils in the development of inflammation and fibrosis. However, little is known about the causal role of eosinophils in intestinal inflammation and especially in intestinal fibrosis. Therefore, in our study, we aimed to investigate the direct effect of eosinophils on fibroblast activation in an in vitro co-culture model. Secondly, we aimed to investigate the impact of eosinophil depletion on intestinal inflammation and fibrosis in a $RAG^{-/-}$ DSS-induced chronic colitis model. This validated model to study intestinal fibrosis lacks a mature adaptive immune system, thereby enabling the examination of the specific impact exerted solely by a functional innate immune system[19].

Results

Activated eosinophils stimulate fibroblast inactivation in an in vitro model

To elucidate the involvement of eosinophils in intestinal fibrosis, we evaluated the direct impact of eosinophils on fibroblast activation. In that context, fibroblasts were co-cultured with or without active eosinophils. Fibroblasts were isolated from the terminal ileum of 3 different patients with fibrostenotic CD and co-cultured with the blood of 3 different non-IBD controls.

Eosinophil activation by rhIL-5 was confirmed during the experiment after 48 and 96 h (Fig. 1A). Additionally, our results demonstrate that eosinophils activated by rhIL-5 exhibit significantly higher activation levels compared to eosinophils that were not treated with rhIL-5 (Fig. 1B).

When fibroblasts isolated from the fibrotic region were co-cultured in the presence of active eosinophils, a reduction of active fibroblasts accompanied by an increase of inactive fibroblasts was observed (both $p=0.001$; Fig. 2A–B). Similarly, co-culture of eosinophils with fibroblasts isolated from unaffected CD tissue resulted in decreased active fibroblasts, but increased inactive fibroblast presence ($p=0.03$ and $p=0.01$, respectively; Fig. 2C–D). However, when eosinophils were not activated by rhIL-5, no increase in inactive fibroblasts nor decrease of active fibroblasts could be observed (both $p=0.5$; Fig. 2E, F). This was further supported by using FAP to differentiate between active and inactive fibroblasts, with no significant differences observed (both

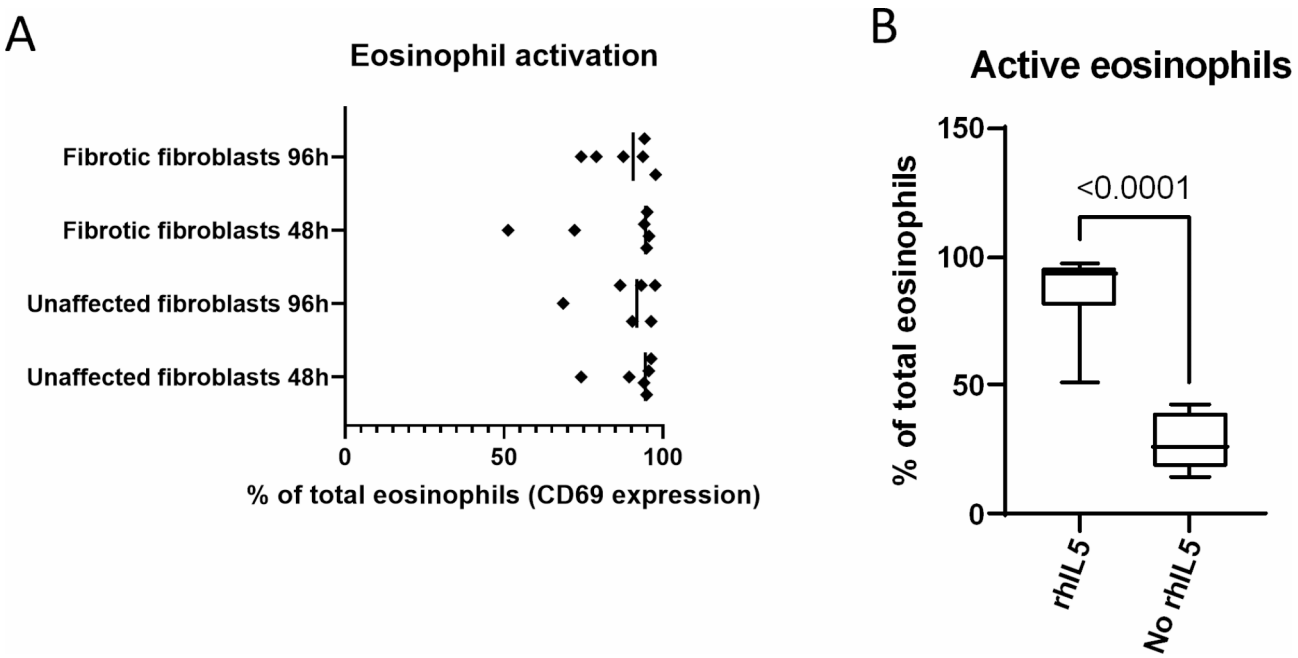

Fig. 1. Eosinophil activation after co-culture with fibroblasts. Eosinophil activation after 24 hours of co-culture with fibroblasts (48 hour and 96-hour timepoint) was confirmed by measuring CD69 expression via flow cytometry (**A**). Eosinophil activation in the presence and absence of rhIL-5 (**B**).

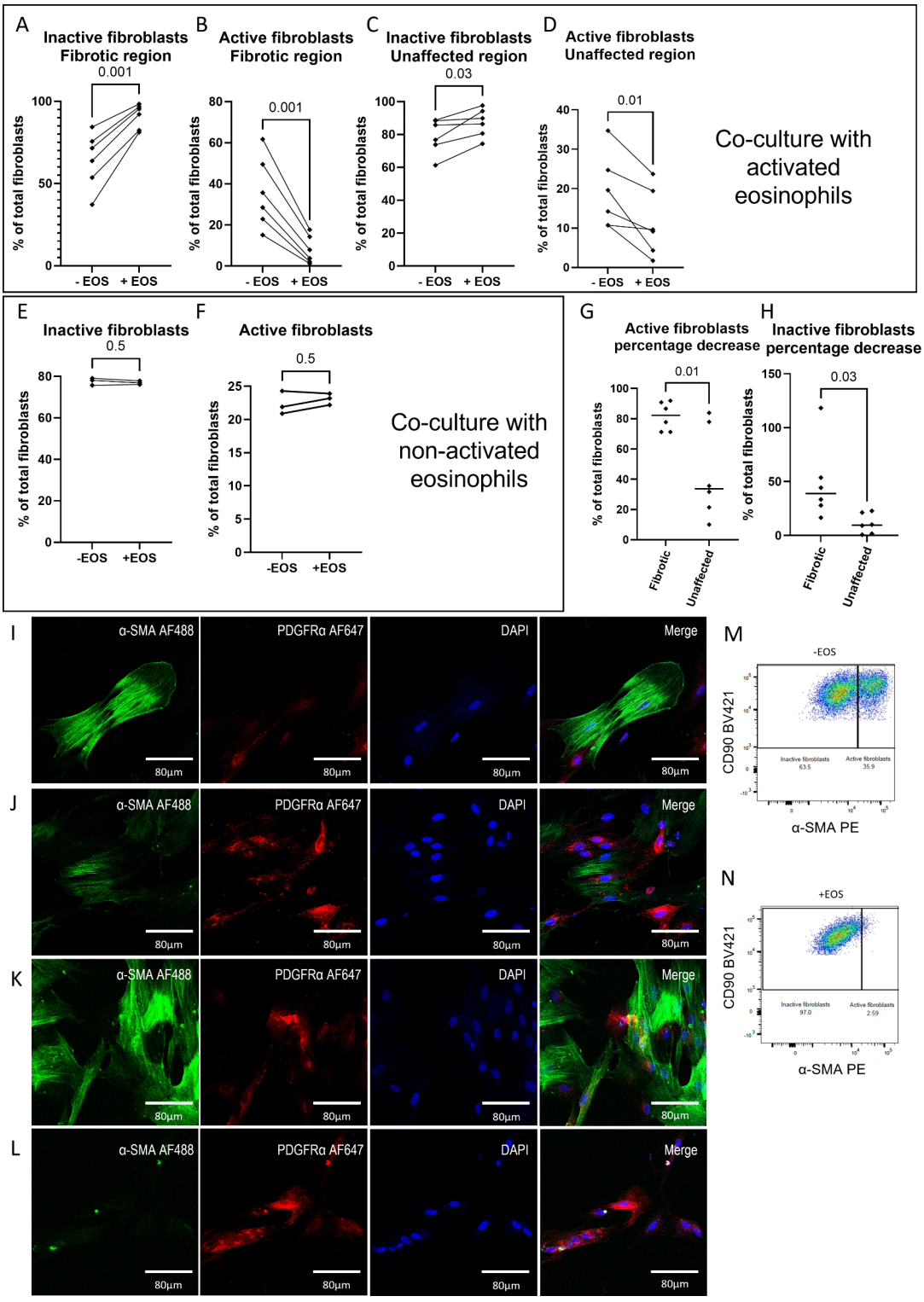

Fig. 2. Eosinophils suppress activation of fibroblastsin vitro. Percentage of inactive fibroblasts and active fibroblasts derived from the unaffected region (**A**, **B**) and fibrostenotic region (**C**, **D**) of CD patients after co-culture with activated eosinophils are depicted. Similarly, the percentage of inactive (**E**) and active (**F**) fibroblasts upon co-culture with non-activated fibroblasts are shown. Percentage decrease of active fibroblasts and inactive fibroblasts are shown as well (**G**, **H**). Similarly, representative immunocytochemical stainings of fibroblasts isolated from the unaffected region cultured without (**I**) and with (**J**) eosinophils are shown. Likewise, fibroblasts isolated from a fibrostenotic region of CD patients were co-cultured without (**K**) and with (**L**) eosinophils. Representative figure of fibroblast activation determined via flow cytometry without (**M**) and with (**N**) co-culturing with activated eosinophils (**M**, **N**). Nuclei were stained by DAPI (blue) as well as α-SMA (green) and PDGFRα (red). $N = 6$ of which 3 biological replicates each with 2 technical replicates.

$p=0.6$; data not shown). Assessing the percentage decrease, this effect was more pronounced in case fibroblasts were isolated from fibrotic CD tissue compared to fibroblasts isolated from unaffected CD tissue (Fig. 2G, H). In line with these observations, we detected decreased α-SMA expression in the conditions where eosinophils were present in the co-culture (Fig. 2I–L). Representative plots of fibroblast activation with and without eosinophil co-culture assessed via α-SMA are represented as well (Fig. 2M, N). Data on eosinophil purity and viability after sorting can be found in supplementary Figs. 1 and 5.

ECP stimulation results in fibroblast inactivation

ECP is produced and secreted by active eosinophils. In order to identify whether this eosinophil-specific mediator could cause similar decreased α-SMA expression, we stimulated fibroblasts isolated from the unaffected region of 3 separate CD patients with ECP. Likewise, we observed a decrease in active fibroblasts and an increase in inactive fibroblasts when fibroblasts were stimulated with ECP ($p=0.04$ and $p=0.03$, respectively; Fig. 3A, B). In line with this, we saw a decrease in α-SMA expression when fibroblasts were stimulated with ECP (Fig. 3C, D). Consistent with previous findings that PDGFRα downregulation is essential for myofibroblast differentiation[20], Fig. 3C shows reduced, but not absent, PDGFRα expression compared to the high levels observed in Fig. 3D.

Eosinophil depletion reduces colitis severity and exacerbates the development of fibrosis

To validate the observed anti-fibrotic effect in an in vivo setting, eosinophils were depleted using a chronic DSS $RAG^{-/-}$ colitis model. Subsequently, we assessed the development of inflammation and fibrosis. The $RAG^{-/-}$ background was chosen to remove any potential interference from the adaptive immune system based on previous studies from our group[19].

We could confirm that ip anti-CCR3 injections depleted both blood and gut eosinophils compared to isotype-injected mice ($p=0.0002$ and $p=0.0003$ respectively; Supplementary Fig. 2). Under non-pathogenic conditions, anti-CCR3 injections did not affect other cell types (Supplementary Table 1). Upon sacrifice, hence after colitis induction, we did not observe a difference in blood and tissue neutrophils, blood and tissue monocytes, tissue macrophages and tissue mast cells between the anti-CCR3 and isotype injected groups (Supplementary Table 2).

To assess colitis development, we determined the total area under the curve (AUC) of the DAI, the macroscopic damage score and histological active disease score. We observed a decrease in total DAI when eosinophils were depleted in mice with colitis compared to the isotype-injected mice ($p=0.0003$) (Fig. 4A, B). Similarly, macroscopic damage scores and microscopic score were lower in the anti-CCR3 compared to the isotype-injected mice ($p=0.002$) that received DSS (Fig. 4C–D). However, no significant differences between the anti-CCR3 and isotype injected group concerning colon weight (Fig. 4E), colon length (Fig. 4F) and colon weight to length ratio (Fig. 4G) was observed (all $p>0.05$). Lastly, eosinophil depletion resulted in a lower histological active disease score ($p=0.006$) (Fig. 4D). Representative H&E-stained slides of eosinophil depleted (Fig. 4H) and isotype injected mice (Fig. 4I) after colitis induction are represented as well.

Total eosinophil count correlated positively with total AUC of the DAI, the macroscopic damage score and the histological active disease score ($R=0.8$ and $p<0.0001$, $R=0.7$ and $p<0.0001$, $R=0.7$ and $p<0.0001$ respectively) (Supplementary Fig. 3). Data are summarized in supplementary Table 3.

Eosinophil depletion resulted in increased collagen deposition ($p=0.005$), assessed by a Martius Scarlet Blue staining (Fig. 5A). Similarly, via a hydroxyproline assay we observed a trend towards increased collagen deposition in the colon when eosinophils were depleted ($p=0.06$) (Fig. 5B). Lastly, there was an increased colonic expression of *COL1A1* when eosinophils were depleted ($p=0.03$) (Fig. 5C). Furthermore, we also observed an increase in collagen expression and deposition in the eosinophil depleted mice under homeostatic conditions (without DSS) ($p=0.03$ and $p=0.002$, respectively) (Fig. 5A, C).

Total eosinophil count correlated moderately and negatively with the collagen deposition determined via MSB staining and hydroxyproline assay and the *Col1a1* mRNA expression (R=-0.5 and $p=0.01$, R=-0.4 and

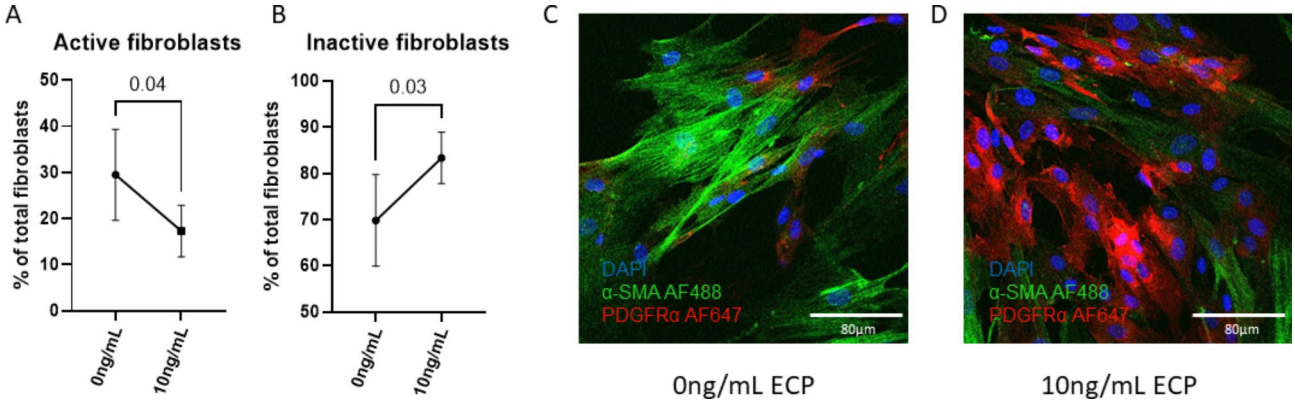

Fig. 3. Stimulation with ECP causes fibroblast inactivation. Flow cytometry results of fibroblast activation (**A**) and inactivation (**B**) after stimulation with ECP. Representative immunocytochemistry without (**C**) and with 10ng/mL ECP stimulation. $N=3$.

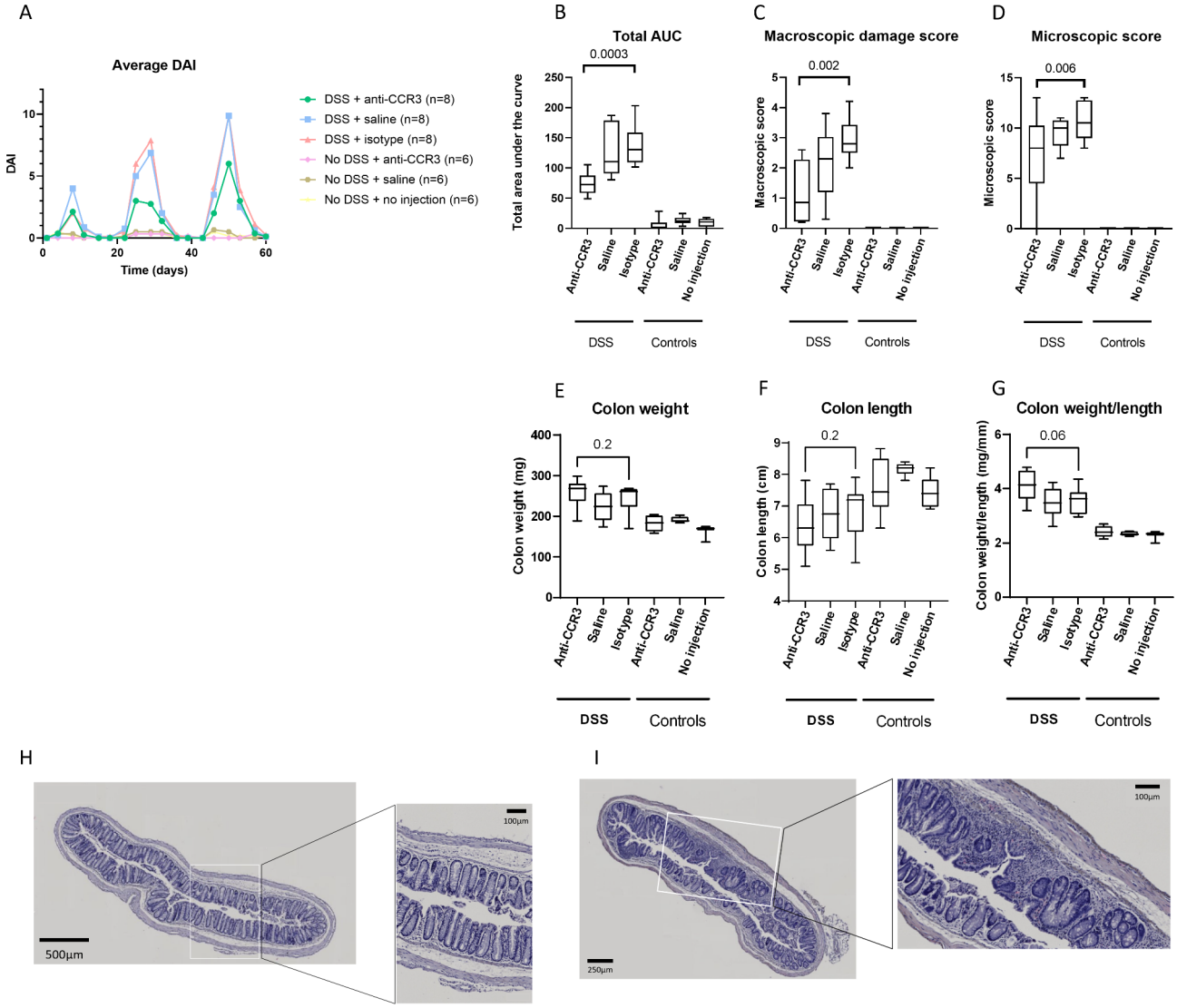

Fig. 4. Eosinophil depletion partially protects from intestinal inflammation. RAG$^{-/-}$ mice in which we introduced colitis via DSS administration showed a lower total AUC of the DAI (**A**, **B**), macroscopic damage score (**C**) and histological active disease score (**D**) after eosinophil depletion compared to control mice. However, no effect on colon weight (**E**), colon length (**F**) and colon weight/length (**G**) was observed. Representative H&E stainings of the eosinophil depleted (**H**) and isotype injected mice (**I**) after colitis induction. DAI = Disease activity index, AUC = area under the curve, DSS = dextran sodium sulphate. $N = 8$ for mice receiving DSS and $N = 6$ for mice not receiving DSS.

$p = 0.05$, R=-0.4 and $p = 0.06$ respectively) (supplementary Fig. 3). Data are summarized in supplementary Table 3.

Immunohistochemical staining combined with second harmonics generation imaging similarly revealed increased collagen deposition in the eosinophil-depleted mice compared to the isotype-injected mice after colitis induction (Fig. 6).

Slides were stained with PDGFRα (red), DAPI (blue) and α-SMA (green) after which they were imaged on a LSM780 NLO confocal microscope that was modified to also enable forward second harmonic generation (fSHG, yellow) imaging. The three immunohistochemical channels were combined with the fSHG channel, which revealed an increased collagen deposition in the anti-CCR3 injected mice (bottom row) in comparison to the isotype injected mice (top row). SHG = second harmonics generation.

Mediators during chronic DSS colitis

In the eosinophil-depleted DSS colitis group, higher levels of IFN-γ, IL-10, IL-1β, FGF-21, and TGF-β3 protein expression were measured compared to the control (isotype injection) group ($p = 0.09$, $p = 0.06$, $p = 0.03$, $p = 0.09$ and $p = 0.06$ respectively) (Fig. 7A–E)). Gene expression of *Il10*, *Il1b*, *and Tgfb3* ($p = 0.07$, $p = 0.04$, and $p = 0.005$) was elevated in the eosinophil-depleted group as well (Fig. 7G, H,J)). No such observations could be made for

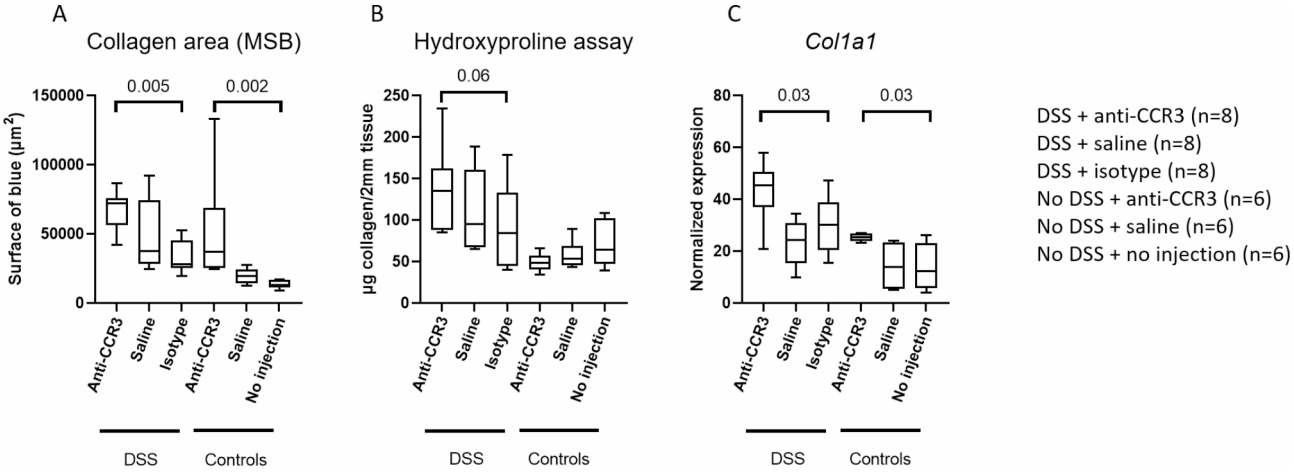

Fig. 5. Eosinophil depletion results in increased collagen deposition and expression. Eosinophil depletion in $RAG^{-/-}$ knockout mice resulted in increased collagen deposition revealed via a Martius Scarlet Blue (**A**) and hydroxyproline assay (**B**). Likewise, increased collagen expression could be found at mRNA level via RT-qPCR (**C**). MSB = Martius Scarlet Blue, DSS = dextran sodium sulphate. $N = 8$ for mice receiving DSS and $N = 6$ for mice not receiving DSS.

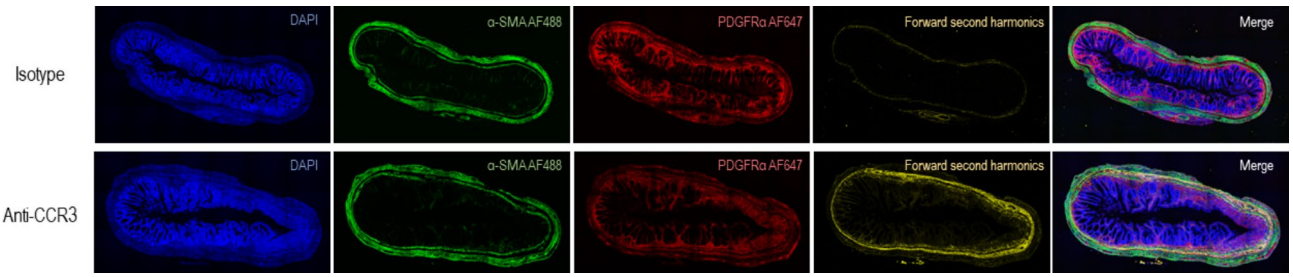

Fig. 6. Eosinophil depletion increases collagen deposition shown by immunohistochemistry and second harmonic generation images. Slides were stained with PDGFRα (red), DAPI (blue) and α-SMA (green) after which they were imaged on a LSM780 NLO confocal microscope that was modified to also enable forward second harmonic generation (fSHG, yellow) imaging. The three immunohistochemical channels were combined with the fSHG channel, which revealed an increased collagen deposition in the anti-CCR3 injected mice (bottom row) in comparison to the isotype injected mice (top row). SHG = second harmonics generation.

Ifng gene expression (Fig. 7F). In contrast, we observed a decrease in *Il1a* in the eosinophil-depleted DSS colitis group compared to the respective control group ($p = 0.01$) (Fig. 7I).

The anti-inflammatory cytokine *Il10* correlated negatively with the inflammation parameters (macroscopic damage score and total AUC of the DAI) but correlated positively with *Col1a1* expression (R=-0.4 and $p = 0.08$, R=-0.4 and $p = 0.05$, $R = 0.5$ $p = 0.03$, respectively). We also observed a trend towards a positive correlation between *Tgfb3* and *Col1a1* expression ($R = 0.5$ and $p = 0.07$), and a significant positive correlation with the hydroxyproline quantification ($R = 0.6$ and $p = 0.007$). Lastly, both IL-1β protein as mRNA expression correlated positively with *COL1A1* expression and collagen deposition (all $R \geq 0.4$ and $p < 0.05$) (data not shown).

Flow cytometry data are summarized in supplementary Tables 2 and protein and gene expression levels can be found in supplementary Table 4.

Discussion

Based on observations in other organ systems, eosinophils have been hypothesized to play a key role in developing inflammation and fibrosis in the gut. However, functional data on the role of eosinophils in inflammation and even more in intestinal fibrosis were lacking[4]. In this study, we observed that co-cultures of activated eosinophils and fibroblasts led to a decrease in active fibroblasts, indicative of anti-fibrotic properties of eosinophils. However, when eosinophils were not activated and co-cultured with fibroblasts, no anti-fibrotic effect could by observed. In a chronic DSS colitis model we observed a pro-inflammatory, but anti-fibrotic role for eosinophils in the intestine at the macroscopic, microscopic, protein and RNA level. Hence, we could not only confirm a functional role for eosinophils in the development of gut inflammation and fibrosis, but we also highlight some potential mediators involved in this pro-inflammatory and anti-fibrotic cascade.

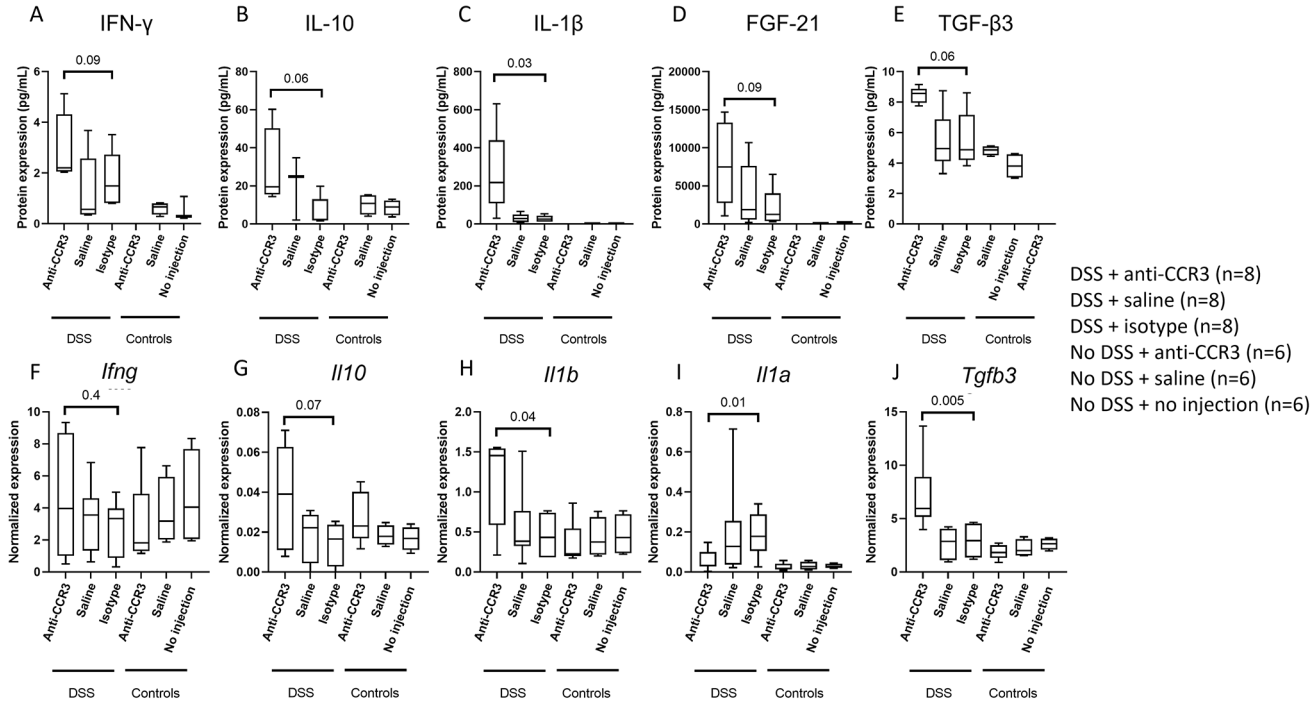

Fig. 7. Eosinophil depleted mice show altered protein and gene expression levels. Protein expression of IFN-γ, IL-10, IL-1β, FGF-21 and TGF-β3 (A-E) and gene expression of IFN-γ, IL-10, IL-1β, FGF-21 and TGF-β3 (F-J), DSS = dextran sodium sulphate. $N = 8$ for mice receiving DSS and $N = 6$ for mice not receiving DSS.

Our data agree with previous studies showing that a genetic deletion of eosinophil major basic protein prevented colitis development[14]. Human studies, albeit more descriptive, similarly pointed to a pro-inflammatory role for eosinophils[9,21–24]. In addition, our data also indicate a protective role for eosinophils in the development of intestinal fibrosis in an in vitro co-culturing model. We demonstrated that eosinophils can induce a transition from active to inactive fibroblasts using a co-culture model. Similarly, the $RAG^{-/-}$ knockout model confirmed an anti-fibrotic role for eosinophils, demonstrated via increased collagen deposition and fibrosis-related gene expression. It is important to note that the anti-fibrotic effect of eosinophils was no longer observed when eosinophils were not activated prior to co-culture. This finding suggests that the impact of eosinophils on fibroblast activation is highly dependent on their activation status. For example, Zagai et al. reported that both eosinophils and ECP increased fibroblast contraction, but several methodological differences may explain the discrepancies with our findings[25]. Notably, we used primary fibroblasts from patients with Crohn's disease and eosinophils from allergic individuals, both factors which could influence fibroblast responses differently compared to Zagai et al.'s use of commercial cell lines and non-activated eosinophils from healthy controls. Additionally, the concentration of ECP and the outcome measures used differed, with our study focusing on fibroblast activation rather than contraction. Lastly, we acknowledge the limitation of exclusively stimulating eosinophils with IL-5. Employing alternative pathways to stimulate eosinophils could potentially yield different outcomes.

Finally, we also observed increased IL-1β and TGF-β3 levels in the eosinophil-depleted DSS mice. Both cytokines have known pro-fibrotic effects[26,27]. Moreover, the IL-1α expression was lower in eosinophil-depleted mice. This observation aligns with expectations since IL-1α is known to be generated by eosinophils and acts to impede the activity of the pro-fibrotic IL-1β[28]. Therefore, the lower IL-1α levels may contribute to enhanced fibrosis upon eosinophil depletion. Although research has primarily focused on the effect of TGF-β1 in fibrosis, and less on TGF-β3, increased TGF-β3 release was shown after in vitro culturing of fibroblasts derived from UC patients during active disease[29]. Another report furthermore demonstrated increased expression of TGF-β3 in human fibrotic lung and liver tissue and showed that blocking of TGF-β3 resulted in the alleviation of fibrosis in a murine model[30]. We thereby identify eosinophil depletion as having a negative impact on fibrosis development potentially by the increased production of IL-1β, which may be explained by the decreased production of the inhibitory IL-1α by the eosinophils. While directing therapeutic attention toward eosinophils holds promise for mitigating inflammatory conditions, this approach should be met with caution so as not to affect wound healing.

Although seemingly in contrast to current literature, in which the general consensus is that eosinophils play a pro-fibrotic role, there also have been some reports indicating a protective role for the eosinophils, even under homeostatic conditions. A study on myocardial infarction in ΔdblGATA1 knockout mice and wild type mice showed increased cell death and fibrosis formation in the mice devoid of eosinophils indicating an anti-fibrotic role for the eosinophils[31]. Eosinophil depletion, again in ΔdblGATA1 knockout mice, furthermore revealed increased intestinal collagen presence under homeostatic conditions as well[32]. Similarly, we also observed increased collagen deposition and *COL1A1* expression when eosinophils were depleted and no colitis

was introduced. This indicates that eosinophils play an important role in dampening fibrotic responses under homeostatic conditions as well.

One of the limitations of our study is that eosinophils were depleted, but not entirely ablated. Therefore, we could potentially observe different results if we used a different model in which eosinophils were completely removed. Furthermore, we deliberately used *RAG*$^{-/-}$ knockout mice, lacking a functioning adaptive immune system, and thereby enabling us to assess whether the adaptive immune system is involved in development of colitis and fibrosis.

To conclude, we identified eosinophils as pro-inflammatory, but antifibrotic cells in an in vitro co-culturing model and confirmed this in a murine DSS colitis model in *RAG*$^{-/-}$ knockout mice. Moreover, we identified this antifibrotic effect on both the protein (collagen deposition via MSB staining, hydroxyproline assay and second harmonics generation imaging) as the gene level (*collagen* expression). We found elevated levels of IFN-γ, IL-10, IL-1β, FGF-21 and TGF-β3, which can potentially contribute to the observed macro- and microscopic findings. Given an increased collagen deposition was also observed in eosinophil depleted mice under homeostatic conditions, eosinophil-depleting therapies may carry a risk of fibrosis development.

Materials and methods

Fibroblast isolation

Fibroblasts were isolated from Crohn's disease patients undergoing surgery due to fibrostricturing disease, in whom we sampled in the most proximal unaffected tissue as well as the fibrotic region of the resection specimen. A single cell suspension was created after which we cultured the fibroblasts in RPMI-5. This medium consists of RPMI-1640 (Gibco, 21875-034) supplemented with 10% fetal bovine serum (FBS) (Gibco, 10270-106), 1% HEPES (Gibco, 15630-056), 1% sodium pyruvate (Gibco, 11360-070), 1% L-glutamine (Gibco, 25030-024) and 1% penicillin streptomycin 10.000I/mL (Gibco, 15140-122). The single cell suspension was cultured for 24 h at 37 °C and 5% CO_2 after which the medium was completely replaced with fresh RPMI-5 resulting in the attachment of only fibroblasts. Fibroblasts were split at least twice before the co-culturing experiment was initiated. Written informed consent was obtained from each patient (S53684). All methods were carried out in accordance with relevant guidelines and regulations. Additionally, all experimental protocols were approved by the University Hospitals of Leuven Ethics Committee Review Board (S53684).

Peripheral blood eosinophil isolation

Peripheral blood eosinophils were isolated from non-IBD controls with an atopic constitution. Therefore, 60mL of blood was sampled after which we performed a red blood cell lysis (NH_4Cl, $KHCO_3$, 0.5 M EDTA; pH 7.4). Cells were washed twice with PBS + 0.5% BSA and centrifuged for 5 min at 400 g. Afterwards, a negative selection was performed for CD2 (Biolegend, 300204) and CD16 (Biolegend, 302004) using 0.5µL of each antibody per 2.10^6 cells. The suspension was incubated on ice for 5 min after which the cells were washed and centrifuged for 5 min at 300 g with 1X MojoSort buffer (Biolegend, 480017). Next, the cells were incubated for 15 min on ice in an appropriate amount of MojoSort™ Streptavidin Nanobeads (Biolegend, 480016). Cells were washed again in MojoSort buffer and centrifuged for 5 min at 300 g. The cells were dissolved in 2.5mL MojoSort buffer, after which they were placed into a magnet for 5 min (Biolegend, 480019). The unlabeled fraction was captured after which the suspension was dissolved at a maximum of 5.10^6 cells per mL. Eosinophils were furthermore sorted on a Sony MA900 based on a high side scatter and high autofluorescence profile (purity > 95%; supplementary Fig. 5).

In vitro co-culturing

After eosinophil isolation, eosinophils were either activated using 0.3ng/mL recombinant human IL-5 (R&D systems, 205-IL-005) or cultured without activation. Several conditions were established; fibroblasts were cultured in RPMI-5 medium only, with the eosinophils activated by rhIL-5 or with the non-activated eosinophils. The eosinophils were activated by recombinant human interleukin-5 (rhIL-5), which was added to the co-culture medium, ensuring continuous stimulation of the eosinophils throughout the duration of the co-culture. Following 24 h of co-culturing, the eosinophil-containing medium was removed and centrifuged at 400 g for 5 min. The resulting supernatant, devoid of eosinophils, was subsequently utilized again. Afterwards, the fibroblasts were cultured for another 24 h. 24 h later, and serving as a second stimulation, eosinophils were isolated again from the same non-IBD control after which co-culture was performed again for 24 h. Eosinophils were then removed as previously described after which the fibroblasts were cultured alone for another 24 h. After a total time period of 96 h, the outcome parameters were determined (supplementary Fig. 4).

Fibroblasts were stained for flow cytometry as described below (single cell staining). Thereby, we assessed fibroblast activation via α-SMA expression based on a Fluorescence minus one (FMO) control. The full fibroblast panel and gating can be found in supplementary Fig. 6 and supplementary Table 5.

Immunocytochemical stainings were performed on the fibroblasts as well, as explained below.

When eosinophils were removed (on day 2 and on day 4 as displayed on supplementary Fig. 4), eosinophil activation was confirmed according to the protocol of the single cell staining. The panel and gating strategy we used can be found in supplementary Fig. 7 and supplementary Table 6.

Immunocytochemical staining

Fibroblasts were seeded at 5000 cells per chamber (Thermofisher, 154534). 24 h later, the cells were fixed with 500µL 100% methanol (Merck, 32213–2.5 L-M) and incubated at -20 °C during 10 min. 500µL wash buffer (PBS (Gibco, 14190-094) + 0.05% Tween-20 (Sigma-Aldrich, P7949-100mL)) per chamber slide was added and incubated for 5 min. This wash step was repeated twice. Afterwards, 500µL of blocking solution (PBS + 1% BSA (Sigma-Aldrich, 9048-46-8)) was added and incubated for 1 h at room temperature. Subsequently, we

added the primary antibodies (supplementary Table 7) and incubated overnight at 4 °C. The following day, the secondary antibody mix was added after a washing step (supplementary Table 7) and incubated for 1 h at room temperature. Afterwards, the slides were washed again and DAPI was added for 10 min at room temperature followed by another washing step (supplementary Table 7). Finally, the slides were mounted and stored at 4 °C until image acquisition.

Fibroblast stimulation

Fibroblasts isolated from the unaffected region of CD patients were stimulated with 10ng/mL ECP (Diagnostics Development, ECP, native) for 48 h after which fibroblast activation was assessed via flow cytometry and immunocytochemistry as described above.

Animal model

Female 6–8 week old RAG$^{-/-}$ knockout C57BL/6 mice were included in our study and were bred at our animal facility. All animals were housed in a semi-specific pathogen free (SPF) facility at the faculty of medicine, Catholic University of Leuven. The RAG$^{-/-}$ knockout C57BL/6 mouse model is a model devoid of the adaptive immune system through which we can specifically study the contribution of the innate immune system. This model was previously established in our group as a suitable model for studying intestinal colitis and fibrosis[19]. Thereby, our group demonstrated the RAG$^{-/-}$ mice to similarly develop chronic intestinal inflammation and fibrosis when compared to wild type mice. Colitis was induced by adding dextran sodium sulphate (DSS) to the drinking water during 3 cycles, in which 1 cycle consisted of 1 week of DSS administration followed by 2 weeks of recovery in which no DSS was added to the drinking water (1.75 − 2.25% − 2.25%) (Fig. 8). Control mice received normal drinking water. Six different groups were created: 3 that received DSS ($n=8$) and 3 that did not receive DSS ($n=6$). The mice receiving DSS were injected with anti-CCR3, saline or isotype, while the mice in which we administered no DSS were treated with anti-CCR3, saline or no injection. In the manuscript we demonstrate the comparison between mice injected with anti-CCR3 in which we induced colitis and mice injected with an isotype and again induced colitis. Therefore, littermates were randomly assigned to the different groups and the mice from these groups were co-housed through the =RAND() function in excel in order to minimize cage effects. The study was approved by and conducted according to the local ethics committee for animal experiments of the Catholic University of Leuven (P205/2020) and in accordance with ARRIVE guidelines.

Mice received 3 DSS cycles of which one cycle consists of 1 week of DSS administration followed by 2 weeks of recovery. Twice weekly the mice received intraperitoneal injections of anti-CCR3, isotype or saline. The DAI was determined at those same timepoints. DAI = disease activity index, DSS = dextran sodium sulphate. $N=8$ for mice receiving DSS and $N=6$ for mice not receiving DSS.

Antibody mediated eosinophil depletion

Twice weekly, mice were intraperitoneally (ip) injected with anti-CCR3, saline or an isotype solution, starting 3 days prior to colitis induction. Eosinophil depletion was achieved via injection of 250 µg anti-CCR3 (clone 6S2-19-4, BE0316, BioXCell). Control injections with saline (362 0204, Braun) or 250 µg isotype (InVivoMAb rat IgG2b isotype control, anti-keyhole limpet hemocyanin, BE0090, BioXCell) were given at the same timepoints.

Evaluation of inflammation and fibrosis

Animals were euthanized with sodium pentobarbital (Vetoquinol), after which blood was taken transorbitally and the distal colon was scored for development of inflammation and fibrosis. Inflammation was scored by using the Disease Activity Index (DAI), macroscopic damage score and histological active disease score. The DAI was determined by assessing body weight loss, stool consistency and presence of blood in the stool as previously described[33]. The histological active disease score was determined on paraffin embedded, 5 µm thick longitudinal and transversal sections and stained with hematoxylin and eosin (H&E) (Langeron's modified Mayer's haemalum, Merck, 1092490500; eosin Y, Merck, HT110216). Briefly, this score comprises the sum of neutrophil infiltration, mononuclear cell infiltration, changes in mucosal architecture, goblet cell loss and

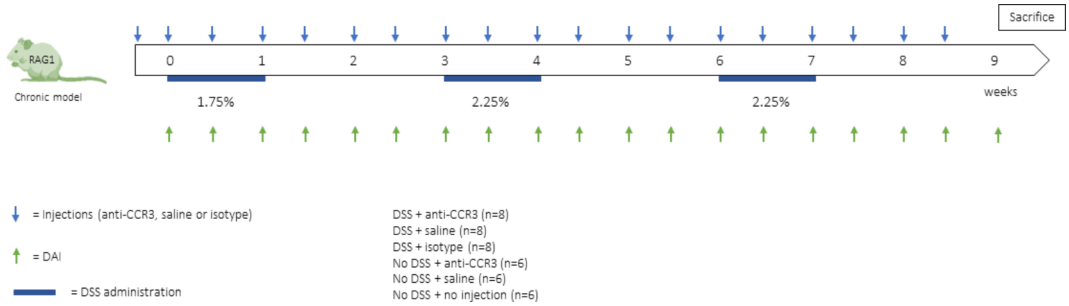

Fig. 8. study design of the chronic DSS model. Mice received 3 DSS cycles of which one cycle consists of 1 week of DSS administration followed by 2 weeks of recovery. Twice weekly the mice received intraperitoneal injections of anti-CCR3, isotype or saline. The DAI was determined at those same timepoints. DAI = disease activity index, DSS = dextran sodium sulphate. $N=8$ for mice receiving DSS and $N=6$ for mice not receiving DSS.

epithelial defects (supplementary Table 8)[34]. The slides were scored by an experienced histopathologist who was blinded to the experimental condition (GDH). Lastly, the macroscopic damage score was determined by the presence of adhesions, hyperemia and length and degree of colon inflammation[35]. Collagen deposition in the colon was additionally assessed via a hydroxyproline assay and a Martius Scarlet Blue (MSB) staining as a measure for fibrosis development as previously described[36]. Lastly, collagen expression was determined by measuring *COL1A1* expression levels via quantitative real time PCR.

Single cell isolation

Colonic tissue was incubated under magnetic stirring for 10 min at 37 °C in RPMI-1640 supplemented with 10% FBS, 1% penicillin streptomycin 10.000U/mL, 5mM EDTA (Invitrogen, 15575-038) and 2% 1 M HEPES to remove mucus and epithelial cells. The epithelial fraction was removed and this step was repeated. Afterwards, the epithelial fraction was discarded and the remaining tissue was cut into smaller fractions. The remaining sample was digested using 10mL Hank's balanced salt solution with Ca^{2+} Mg^{2+} (Gibco, 24020-117) supplemented with 10 mg/mL collagenase type 4 (Worthington, LS004188), 0.2% DNase I (Roche, 10104159001) and 2% 1 M HEPES at 37 °C for 50 min to 1 h. The isolated single cell fraction was filtered through a 70 µm cell strainer (Greiner Bio-one, 542070), after which the cells were counted and used for flow cytometry.

Single cell staining

Next, single cells were stained for fixable viability dye 780 (Invitrogen, 65-0865-14) for 25 min at room temperature and protected from light. Cells were washed with PBS + 0.5% BSA and centrifuged for 5 min at 400 g. The supernatant was discarded and the pellet was dissolved in blocking mix (2% inactivated serum in PBS + 0.5% BSA) for 10 min at 4 °C. Single cells were washed and centrifuged again and incubated in the antibody mixes (supplementary Table 9) for 30 min at 4 °C. Similarly, whole blood was incubated in the antibody mixes (supplementary Table 9) after which a red blood cell lysis (1X) (10X = 1.5 M NH_4Cl, 100mM $KHCO_3$, 10mM disodium EDTA in 100mL H_2O; pH 7.4) was performed for 10 min. Blood was centrifuged for 5 min at 400 g after which the cells were washed with PBS + 0.5% BSA. Afterwards, both peripheral blood as intestinal cells were washed again and incubated in 1% PFA (Merck, 30525-89-4) for 15 min at room temperature. Once more, cells were washed with PBS + 0.5% BSA + 2mM EDTA and stored in 4 °C until acquisition.

Gating strategy can be found in supplementary Fig. 8.

Samples were acquired on a BD LSR Fortessa. Quality control was performed before each acquisition by using FACS Diva™ CS&T research beads (BD, 655051). For fluorescence compensation settings anti-rat/anti-hamster Ig,κ CompBeads (BD, 51-90-9000949) or anti-mouse Ig,κ CompBeads (BD, 51-90-9001229) were used. Fluorescence minus one (FMO) controls were included. Flow cytometry files were analyzed using the BD FlowJo software.

Protein measurement

0.5 cm colonic tissue was incubated for 24 h in RPMI-1640 supplemented with 10 FBS and 1% penicillin streptomycin 10.000U/mL at 37 °C. Afterwards, the medium was collected and centrifuged for 5 min at 10,000 rpm after which supernatant was removed and stored in -80 °C.

TNF-α, IFN-γ, IL-1β, IL-4, IL-5, IL-6, IL-8, IL-10, IL-12p40, IL-12p70, IL-13, IL-22, IL-33, VEGF-A, MIP-1α, MIP-3α, MMP-9, IP-10, FGF21 and TGF-β1,2,3 protein levels were measured with the MSD® U-plex system according to the manufacturer's guidelines (MesoScale Discovery).

Quantitative real time PCR

Total RNA was extracted from snap frozen colon (Qiagen RNeasy mini kit, Cat #74106) after which 1 µg was reverse transcribed using 500U MultiScribe Reverse Transcriptase (Thermofisher) at 37 °C for 120 min. RT-qPCR was performed for *COL1A1*, *IL-1α*, *IFN-γ*, *IL-10*, *IL-1β*, *FGF-21 and TGF-β3* with *β-actin* and *GAPDH* as housekeeping genes on a CFX Connect Real-Time PCR detection System (Bio-Rad). Standard was performed in triplicate and samples in duplicate.

Immunohistochemical staining and second harmonics generation imaging

Tissue samples were processed and embedded in paraffin (supplementary Table 10). Subsequently, 5 µm-thick slides were cut. The slides were then de-paraffinized using the following steps: they were first incubated twice for 3 min in HistoChoice clearing agent (Sigma Aldrich, H2779), then for 3 min in 50% HistoChoice-ethanol, twice for 3 min in 100% ethanol (Merck, 64-17-5), 3 min in 95% ethanol, 3 min in 70% ethanol, 3 min in 50% ethanol, and 3 min in demineralized water.

For antigen retrieval, the slides were treated with a sodium citrate buffer (10mM sodium citrate, Merck, 61-32-04-3, 0.05% Tween 20, Sigma-Aldrich, P9416, pH 9.0) at 95 °C for 20 min. Following this, the slides were permeabilized with 0.3% Triton™ X-100 (Sigma-Aldrich, 9036-19-5) and 0.3 M glycine (Merck, 56-40-6) in PBS for 10 min, and then blocked with 1% BSA in PBS-Tween20 for 1 h.

For immunostaining, primary antibodies (Supplementary Table 11) were incubated overnight at 4°C. The next day, the slides were washed three times with PBS-Tween20 for 5 minutes each. Secondary antibodies were added and left to incubate for 1 hour at room temperature, protected from light (supplementary Table 11). After another wash with PBS-Tween20 for 10 minutes, autofluorescence quenching was performed following the manufacturer's guidelines (VectorLaboratories, SP-8400-15). To label cell nuclei, 4', 6-diaminido-2-phenylindole (DAPI) was added at room temperature for 15 min (supplementary Table 11), followed by a final wash with PBS-Tween20 for 10 min. Finally, the slides were mounted and sealed using Vector Laboratories (SP-8400-15). Immunohistochemically stained slides were then analyzed via ImageJ.

Second harmonic generation imaging was used to visualize the collagen structures[37]. Images were captured with a 25x water immersion objective (0.8 NA, Zeiss) on a LSM 780 confocal microscope (Carl Zeiss Microscopy). A tuneable Mai Tai Titanium-Sapphire DS (Spectra Physics) pulsed femtosecond laser was used as an illumination source, and second harmonics were elicited at 850 nm. The SHG signals were recorded in the forward direction on a non-descanned detector (BIG, Zeiss).

Statistical analysis

GraphPad prism 9.4.0 was used to perform statistical analysis. Normality was determined using a Shapiro–Wilk test, after which an unpaired analysis (unpaired t-test or Mann–Whitney analysis) was performed. Correlations were assessed using the Pearson correlation coefficient (for parametric data) or the nonparametric Spearman correlation. Data are presented as median (interquartile range).

Data availability

The data underlying this article will be shared on reasonable request to the corresponding author.

Received: 19 March 2024; Accepted: 1 November 2024
Published online: 07 November 2024

References

1. De Souza, H. S. P. & Fiocchi, C. Immunopathogenesis of IBD: Current state of the art. *Nat. Rev. Gastroenterol. Hepatol.* **13**, 13–27 (2016).
2. Herrera, J. et al. Extracellular matrix as a driver of progressive fibrosis. *J. Clin. Invest.* **128**, 45–53 (2018).
3. Yoo, J. H., Holubar, S. & Rieder, F. Fibrostenotic strictures in Crohn's disease. *Intest Res.* **18**, 379–401 (2020).
4. Jacobs, I. et al. Role of eosinophils in intestinal inflammation and fibrosis in inflammatory bowel disease: An overlooked villain? *Front. Immunol.*, vol. 12 (2021). Preprint at https://doi.org/10.3389/fimmu.2021.754413
5. Mir, A. et al. Elevated serum eotaxin levels in patients with inflammatory bowel disease. *Am. J. Gastroenterol.* **97**, 1452–1457 (2002).
6. Coppi, L. C. et al. Comparative study of eosinophil chemotaxis, adhesion, and degranulation in vitro in ulcerative colitis and Crohn's disease. *Inflamm. Bowel Dis.* **13**, 211–218 (2007).
7. Geboes, K. et al. A reproducible grading scale for histological assessment of inflammation in ulcerative colitis. *Gut* **47**, 404–409 (2000).
8. McBrien, C. N. & Menzies-Gow, A. The biology of eosinophils and their role in asthma. *Front. Med. (Lausanne)* **4**, 93 (2017).
9. Amcoff, K. et al. Prognostic significance of faecal eosinophil granule proteins in inflammatory bowel disease. *Scand. J. Gastroenterol.* **54**, 1237–1244 (2019).
10. Wędrychowicz, A. et al. Clinical value of serum eosinophilic cationic protein assessment in children with infflammatory bowel disease. *Archives Med. Sci.* **10**, 1142–1146 (2014).
11. Abedin, N. et al. Fecal eosinophil cationic protein is a diagnostic and predictive biomarker in young adults with inflammatory bowel disease. *J. Clin. Med.* **8**, 2025 (2019).
12. Lampinen, M. et al. IL-5 and TNF-α participate in recruitment of eosinophils to intestinal mucosa in ulcerative colitis. *Dig. Dis. Sci.* **46**, 2004–2009 (2001).
13. Sugimoto, K. et al. Improvement in ulcerative colitis by administration of benralizumab for comorbid refractory bronchial asthma: A novel clinical observation. *Inflamm. Bowel Dis.* **27**, E3–E4 (2021).
14. Furuta, G. T. et al. Eosinophils alter colonic epithelial barrier function: Role for major basic protein. *Am. J. Physiol. Gastrointest. Liver Physiol.* **289**, 890–897 (2005).
15. Colon, S. et al. Peroxidasin and eosinophil peroxidase, but not myeloperoxidase, contribute to renal fibrosis in the murine unilateral ureteral obstruction model. *Am. J. Physiol. Ren. Physiol.* **316**, 360–371 (2019).
16. Masterson, J. C. et al. Eosinophils and IL-33 perpetuate chronic inflammation and fibrosis in a pediatric population with stricturing Crohn's ileitis. *Inflamm. Bowel Dis.* **21**, 2429–2440 (2015).
17. Takemura, N. et al. Eosinophil depletion suppresses radiation-induced small intestinal fibrosis. *Sci. Transl Med.* **10**, 1–8 (2018).
18. Pégorier, S., Wagner, L. A., Gleich, G. J. & Pretolani, M. Eosinophil-derived cationic proteins activate the synthesis of remodeling factors by airway epithelial cells. *J. Immunol.* **177**, 4861–4869 (2006).
19. Creyns, B. et al. Fibrogenesis in chronic murine colitis is independent of innate lymphoid cells. *Immun. Inflamm. Dis.* **8**, 393–407 (2020).
20. Yao, L. et al. Temporal control of PDGFRα regulates the fibroblast-to-myofibroblast transition in wound healing. *Cell. Rep.* **40**, (2022).
21. Carlson, M., Raab, Y., Peterson, C., Hällgren, R. & Venge, P. Increased intraluminal release of eosinophil granule proteins EPO, ECP, EPX, and cytokines in ulcerative colitis and proctitis in segmental perfusion. *Am. J. Gastroenterol.* **94**, 1876–1883 (1999).
22. Carvalho, A. T. P. et al. Immunohistochemical study of intestinal eosinophils in inflammatory bowel disease. *J. Clin. Gastroenterol.* **36**, 120–125 (2003).
23. Woodruff, S. A., Masterson, J. C., Fillon, S., Robinson, Z. D. & Furuta, G. T. Role of eosinophils in inflammatory bowel and gastrointestinal diseases. *J. Pediatr. Gastroenterol. Nutr.* **52**, 650–661 (2011).
24. Roca, M. et al. Fecal calprotectin and eosinophil-derived neurotoxin in healthy children between 0 and 12 years. *J. Pediatr. Gastroenterol. Nutr.* **65**, 394–398 (2017).
25. Zagai, U., Sköld, C. M., Trulson, A., Venge, P. & Lundahl, J. The effect of eosinophils on collagen gel contraction and implications for tissue remodelling. *Clin. Exp. Immunol.* **135**, 427–433 (2004).
26. Kolb, M., Margetts, P. J., Anthony, D. C., Pitossi, F. & Gauldie, J. Transient expression of IL-1β induces acute lung injury and chronic repair leading to pulmonary fibrosis. *J. Clin. Invest.* **107**, 1529–1536 (2001).
27. Wilson, M. S. et al. Bleomycin and IL-1β-mediated pulmonary fibrosis is IL-17A dependent. *J. Exp. Med.* **207**, 535–552 (2010).
28. Borthwick, L. A. The IL-1 cytokine family and its role in inflammation and fibrosis in the lung. *Seminars in Immunopathology*, vol. 38 517–534 (2016). Preprint at https://doi.org/10.1007/s00281-016-0559-z
29. McKaig, B. C., Hughes, K., Tighe, P. J. & Mahida, Y. R. Differential expression of TGF-beta isoforms by normal and inflammatory bowel disease intestinal myofibroblasts. *Am. J. Physiol. Cell. Physiol.* **282**, 172–182 (2002).
30. Sun, T. et al. F I B R O S I S TGFβ2 and TGFβ3 isoforms drive fibrotic disease pathogenesis. *Sci. Transl Med.* **13** (2021). https://www.science.org
31. Liu, J. et al. Eosinophils improve cardiac function after myocardial infarction. *Nat. Commun.* **11**, (2020).
32. Ignacio, A. et al. Small intestinal resident eosinophils maintain gut homeostasis following microbial colonization. *Immunity* **55**, 1250–1267e12 (2022).

33. Egger, B. et al. Characterisation of acute murine dextran sodium sulphate colitis: Cytokine profile and dose dependency. *Digestion* **62**, 240–248 (2000).
34. Breynaert, C. et al. Unique gene expression and MR T2 relaxometry patterns define chronic murine dextran sodium sulphate colitis as a model for connective tissue changes in human Crohn's disease. *PLoS ONE* **8**, (2013).
35. Eken, A., Singh, A. K., Treuting, P. M. & Oukka, M. IL-23R + innate lymphoid cells induce colitis via interleukin-22-dependent mechanism. *Mucosal Immunol.* **7**, 143–154 (2014).
36. Forkel, M. et al. Distinct alterations in the composition of mucosal innate lymphoid cells in newly diagnosed and established Crohn's disease and ulcerative colitis. *J. Crohns Colitis* **13**, 67–78 (2019).
37. Cicchi, R. & Pavone, F. S. *Probing Collagen Organization: Practical Guide for Second-Harmonic Generation (SHG) Imaging*, vol. 1627 (Springer New York, 2017).

Acknowledgements

This research has been funded by an internal C1 project (ZKD2906 – C14/17/097) of KU Leuven. TV is supported by a senior clinical research fellowship of the Flanders Research Foundation (FWO Vlaanderen; 1830517 N). BV and CB are supported by the Clinical Research Fund (KOOR) at the University Hospitals Leuven. BV is also supported by the Research Council at the KU Leuven. SV holds a BOF-FKO from the KU Leuven. SHG signals were recorded on a Zeiss LSM 780 – SP Mai Tai HP DS (Cell and Tissue Imaging Cluster (CIC), Supported by Hercules AKUL/11/37 and FWO G.0929.15 to PVB, KU Leuven).We extend our gratitude to Ingrid De Meester of the University of Antwerp for kindly providing the FAP FITC antibody used in this study.

Author contributions

Study concept and design: IJ, TV, BV. Histological scoring: GDH. Data acquisition and analysis: IJ, SD, JC, ED, BJK. Interpretation of data: IJ, JC, BJK, ED, TM, PVB, GM, SV, CB, TV, BV. Writing the initial manuscript: IJ. Supervision: TV and BV. All authors approved the final version of the manuscript.

Declarations

Competing interests

TV has received research support, lecture and consultancy fees from Takeda. BV reports research support from AbbVie, Biora Therapeutics, Landos, Pfizer, Sossei Heptares and Takeda; speaker's fees from Abbvie, Biogen, Bristol Myers Squibb, Celltrion, Chiesi Falk, Ferring, Galapagos, Janssen, Lily, MSD, Pfizer, R-Biopharm, Sandoz, Takeda, Tillots Pharma, Truvion and Viatris; consultancy fees from Abbvie, Almentiv, Applied Strategic, Atheneum, BenevolentAI, Biora Therapeutics, Bristol Myers Squibb, Galapagos, Guidepoint, Landos, Lily, Mylan, Inotrem, Ipsos, Janssen, Prifer, Progenity, Sandoz, Santa Ana Bio, Sosei Heptares, Takeda, Tillots Pharma and Viatris. SV receives financial support for research from AbbVie, J&J, Pfizer, Takeda and Galapagos; receives speakers' and consultancy fees from AbbVie, AbolerIS Pharma, AgomAb, Alimentiv, Arena Pharmaceuticals, AstraZeneca, Avaxia, BMS, Boehringer Ingelheim, Celgene, CVasThera, Cytoki Pharma, Dr Falk Pharma, Ferring, Galapagos, Genentech-Roche, Gilead, GSK, Hospira, Imidomics, Janssen, J&J, Lilly, Materia Prima, MiroBio, Morphic, MrMHealth, Mundipharma, MSD, Pfizer, Prodigest, Progenity, Prometheus, Robarts Clinical Trials, Second Genome, Shire, Surrozen, Takeda, Theravance, Tillots Pharma AG, Zealand Pharma. GDH receives fees for his activities as central pathology reader from Centocor and receives speakers' fees from Janssen. CB has received research fees from Ablynx. All other authors do not have any interest to disclose. Other authors to not have any interest to disclose.

Additional information

Supplementary Information The online version contains supplementary material available at https://doi.org/10.1038/s41598-024-78602-0.

Correspondence and requests for materials should be addressed to B.V.

Reprints and permissions information is available at www.nature.com/reprints.

Publisher's note Springer Nature remains neutral with regard to jurisdictional claims in published maps and institutional affiliations.